photonics

MDPI

Article

Design of Filterless Horseshoe Networks Optimized for Interoperable Coherent Pluggable Transceivers

Federica Gatti [1,*], João Pedro [1,2], Nelson Costa [1] and Luís Cancela [2,3]

[1] Nokia, Optical Networks, 2790-078 Carnaxide, Portugal
[2] Instituto de Telecomunicações, Instituto Superior Técnico, 1049-001 Lisboa, Portugal
[3] Department of Information Science and Technology, Iscte—Instituto Universitario de Lisboa, 1649-026 Lisboa, Portugal
* Correspondence: federica.gatti@nokia.com

Abstract

The continuous growth of traffic in metro networks is increasing the need for cost-effective, scalable, and power-efficient optical solutions. Filterless optical networks (FONs) have emerged as a promising architecture for metro-aggregation and metro-access domains, thanks to their low complexity and reliance on passive optical components. However, their inherent broadcast nature introduces key challenges, including spectrum waste, limited power equalization, and significant noise accumulation, particularly when coherent pluggable transceivers are employed. This work provides a detailed assessment of FON performance using state-of-the-art multi-source agreement (MSA)-compliant coherent modules, evaluating both point-to-point (P2P) and digital subcarrier multiplexing (DSCM)-based point-to-multipoint (P2MP) architectures. A novel optical amplifier (OA) optimization algorithm is proposed to balance expressed and added signal power in FON, accounting for optical power saturation effects and optical performance degradation due to limited power at the receiver input. The analysis highlights the substantial impact of transmitter out-of-band (OB) noise in FONs and its detrimental accumulation during multi-channel colorless aggregation, which can limit network capacity. In scenarios with lower capacity requirements, P2MP architectures demonstrate superior performance, benefiting from reduced insertion loss and lower OB noise accumulation while offering enhanced scalability compared with P2P solutions. Overall, the study highlights that FONs combined with coherent pluggables can support cost-efficient and scalable metro solutions, provided that OB noise, power imbalance, and amplifier operation are properly addressed through optimized design strategies.

Keywords: filterless network; optical amplification; coherent pluggable transceiver; network optimization

Received: 19 February 2026
Revised: 6 March 2026
Accepted: 9 March 2026
Published: 12 March 2026

1. Introduction

Advancements in 5G, artificial intelligence (AI), augmented reality (AR) and virtual reality (VR), among others, are leading to an exponential increase in data consumption [1,2] resulting in an increase in total global network traffic, with a projection of a compound annual growth rate (CAGR) through 2033 of 18–27% [2]. Optical metro networks will play a pivotal role in this evolution [3]. However, both metro-aggregation [4] and metro-access [5] network segments are very cost-sensitive. Thus, it is essential to adopt cost-effective future-proof architectures in these networks, which have low-cost and can scale to accommodate demand growth.

Deploying optical networks that employ simple passive optical components, such as couplers and splitters, instead of more expensive optical switches and optical add-drop multiplexers (OADM), has the potential to significantly reduce cost. Given the small size of metro-aggregation and metro-access networks and the introduction of coherent-detection-based transceivers in these segments, filterless optical networks (FONs) become a promising architecture to cost-effectively meet operators' requirements [5,6]. Since these networks mainly perform traffic distribution/aggregation functions, the traffic pattern is mostly hub-and-spoke and determines the network architecture, which typically comprises a few higher-capacity central (hub) nodes and a larger number of lower-capacity distributed (leaf) nodes, often arranged in a horseshoe physical topology. FONs have also been demonstrated to be a suitable architecture for point-to-multipoint (P2MP) transmission via digital subcarrier multiplexing (DSCM) [7], which can further reduce capital expenditure (CAPEX) compared to point-to-point (P2P) architecture [8]. Indeed, while P2P transceivers transmit and receive the same data rate at the two ends of the link, requiring paired transceivers at hub and leaf nodes, DSCM-P2MP transceivers efficiently handle the intrinsic capacity imbalance between hub and leaf nodes, as they allow the use of a single high-capacity device at the hub node serving multiple leaf nodes equipped with low-capacity transceivers [4,9].

When compared to traditional filtered architectures, some potential drawbacks of FONs have to be carefully assessed, such as (i) the spectrum waste, (ii) limited optical power equalization at intermediate nodes, and (iii) increased impact of noise. This latter effect, when combined with the fact that channels are not filtered out in FON nodes, also leads to potential optical power limitations in optical amplifiers (OAs), i.e., the saturation power level of OAs is more easily reached. Spectrum waste is a consequence of the broadcast nature of splitters used in the filterless nodes. However, the recent availability of high-capacity and cost-effective coherent pluggable interfaces, e.g., based on different multi-source agreement standards (MSAs) such as Open ZR+ [10], Open ROADM [11] and Open XR [12], and the fact that metro-aggregation networks typically feature a hub-and-spoke traffic pattern, limiting the importance of spectrum reuse in non-overlapping paths, suggest that this may not be a relevant drawback in this particular scenario [4].

Limited optical power equalization in filterless nodes can lead to a noticeable power imbalance between expressed and added signals. This effect results in enhanced complexity in managing the optical power of each individual channel at the receiver input. Moreover, the combined effect of overlapping signals and noise with different origins and potentially different optical power levels leads to an enhancement of the impact of noise in the channels transmitted with lower power levels, thus significantly impacting their quality of transmission (QoT), when compared to channels transmitted with higher optical power. Hence, the placement of OAs and the optimization of their settings must be customized to cater for the highlighted specifics of FONs, demanding methodologies that differ from the ones utilized with filtered architectures. Amplified spontaneous emission (ASE) noise is added into the FON every time an optical amplifier (OA) is used. The noise introduced by transmitters (Tx) is also critical in FONs. This noise source comprises two spectral components: the Tx in-band (IB) noise, within the spectrum of the optical signal generated, and the Tx out-of-band (OB) noise, in the remaining transmission bandwidth. The OB noise is significantly suppressed in filtered networks, but not in the case of FONs. Particularly, it will propagate along the downstream links, and it has a cumulative impact, since whenever multiple signals are colorlessly aggregated, the OB noise from each added signal degrades the optical signal-to-noise ratio (OSNR) of the other jointly added signals. Figure 1 illustrates how individual OB noise affects other signals once they are aggregated. Similarly, every time a new signal is added in the upstream (US) direction (using the same

optical fiber), the downstream (DS) channels are also impacted. Moreover, as dropped channels are not blocked at intermediate nodes, all existing DS channels will impact the US ones when they are added.

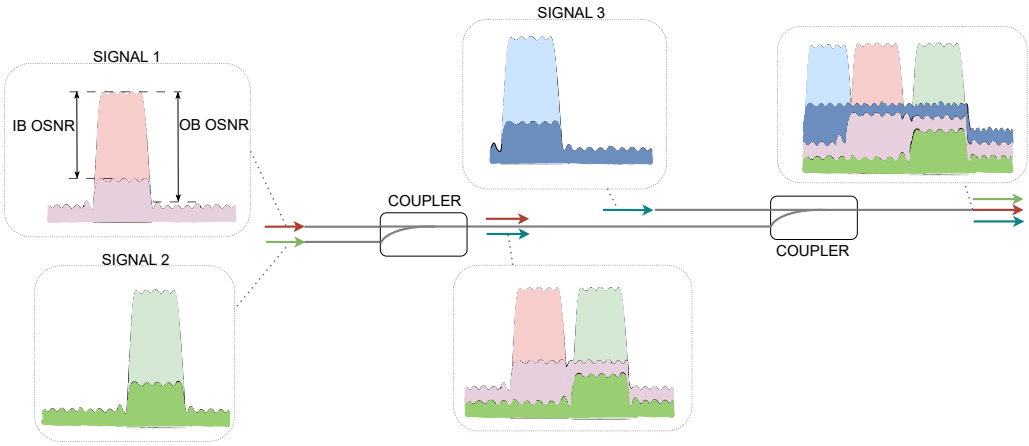

Figure 1. Illustration of IB and OB noise accumulation when aggregating three different signals (distinguished by pink, green, and blue colors) in a FON.

This work provides insight on the design challenges in FONs when using high-capacity and interoperable coherent pluggable transceivers both in a low- and high-capacity scenario and proposes a methodology to optimize OA settings so as to maximize the likelihood of finding feasible designs when considering both downstream and upstream transmission directions. Moreover, the analysis covers not only the cases of P2P transmission but also the utilization of P2MP coherent pluggable transceivers. The simulation results validate the importance of adopting a customized algorithm for setting the OAs, show that deploying higher-performing coherent pluggable transceivers is key in FONs, and highlight the performance benefits of using P2MP devices.

The remainder of the article is organized as follows. Section 2 provides a state-of-the-art overview of the existing FON architectures and introduces P2P and P2MP transmission with coherent pluggable optical transceivers, highlighting the key characteristics of the available MSAs. Section 3 details the network scenario considered and proposes an OA optimization methodology customized for this scenario. Section 4 presents and discusses the most relevant simulation results, providing insight on the scalability of FONs when combined with coherent pluggable transceivers. Finally, Section 5 draws the main conclusions of this work.

2. State-of-the-Art Review

2.1. Filterless Optical Networks

FONs reduce or avoid the need for active photonic reconfigurable components within the optical line system [13]. In this case, the use of wavelength-selective switches (WSSs) in OADMs is replaced by passive optical splitters and combiners to manage the fiber interconnections and add/drop of channels. This much simpler architecture reduces the initial installation cost (CAPEX) of the network, as well as the operational expenditure (OPEX). Thanks to these advantages, FONs supporting P2P coherent transceivers have been extensively investigated in recent years. A comprehensive overview of the first decade of research on FONs is available in [13,14]. Moreover, studies assessing FON performance in metropolitan core and aggregation networks, as well as comparative analyses against conventional metro architectures based on active switching, are reported in [15–17]. An overview of FON limitations and a techno-economic study has been presented in [18], highlighting future research directions.

Because signals are broadcast and no optical filtering is applied at both end and intermediate nodes (following the so-called drop-and-waste transmission), channels propagate onto links where they are not needed, leading to unnecessary spectrum waste. This limitation has been taken into account in the routing and spectrum assignment (RSA) problem presented in [19], and solutions such as programmable FON (PFON) have been proposed to mitigate it [20–22]. Design optimization approaches have also already been investigated, focusing on strategic placement of OAs, the adoption of higher-order modulation formats, and the reduction in the number of transponders while maximizing network QoT, as discussed in [5,23]. Dedicated optical-layer path protection strategies have been proposed in [24–26]. Moreover, some works have proposed the adoption of semi-filterless designs, particularly for larger networks, by diving the network into filterless sub-networks and installing filters at boundary nodes [27–29].

FONs can also further reduce CAPEX when utilized with novel DSCM-based P2MP coherent pluggable transceivers, since this combination allows for significant transceiver savings when compared to using traditional P2P coherent devices. Several works have addressed this scenario, highlighting the said benefits but also the particular constraints that need to be accounted for in the network design stage, such as the maximum allowed power imbalance between the subcarriers reaching the receiver at the hub node [4,9]. In the metro-aggregation segment, the greater flexibility of DSCM-based coherent modules has been shown to lead to significant cost savings [30], which can be augmented by reducing the number of OAs via carefully selecting their placement [31,32] and more accurately modeling the impact of non-linear fiber transmission effects [33]. Despite the thoroughness and detail of the aforementioned optimization studies, the impact of transmitter OB noise has largely been ignored or not modeled in some of these studies. However, its detrimental accumulation across the network has a significant impact, which can be of comparable magnitude to that of the ASE noise introduced by OAs, as will be shown in this work.

2.2. Point-to-Point and Point-to-Multipoint Coherent Transceivers

As stated, both metro-access and metro-aggregation networks frequently adopt a horseshoe topology, featuring two hub nodes and several leaf nodes between. This topology is suitable to support a hub-and-spoke traffic pattern and ensure survivability to single link and hub failures, while requiring the minimum amount of optical fiber. In the metro-access scenario, low-speed traffic originating from fixed networks and radio access networks (RANs) is merged in leaf nodes with enterprise traffic at provider edge routers (PERs), creating a typically low-capacity signal of 10/25G [30]. This signal is then connected to provider routers (PR) in hub nodes [30]. In this scenario, there is a large imbalance between the capacity needed in the hub nodes and that required at each leaf node.

The concept of P2MP coherent optical networks based on DSCM technology has been proposed to overcome this limitation [7]. In this case, the Tx creates channels in the digital domain—the digital subcarriers (SCs)—where each SC or subset of SCs can be viewed and handled as an independent channel, and the receiver (Rx) digitally demultiplexes the SCs assigned to that Rx only. Figure 2 illustrates the paradigm shift from P2P towards P2MP architecture: the former relies on pairing transceivers at the hub and leaf nodes, resulting in a large number of transceivers at hub nodes, while the latter uses a few or even just a single high-capacity transceiver at each hub node.

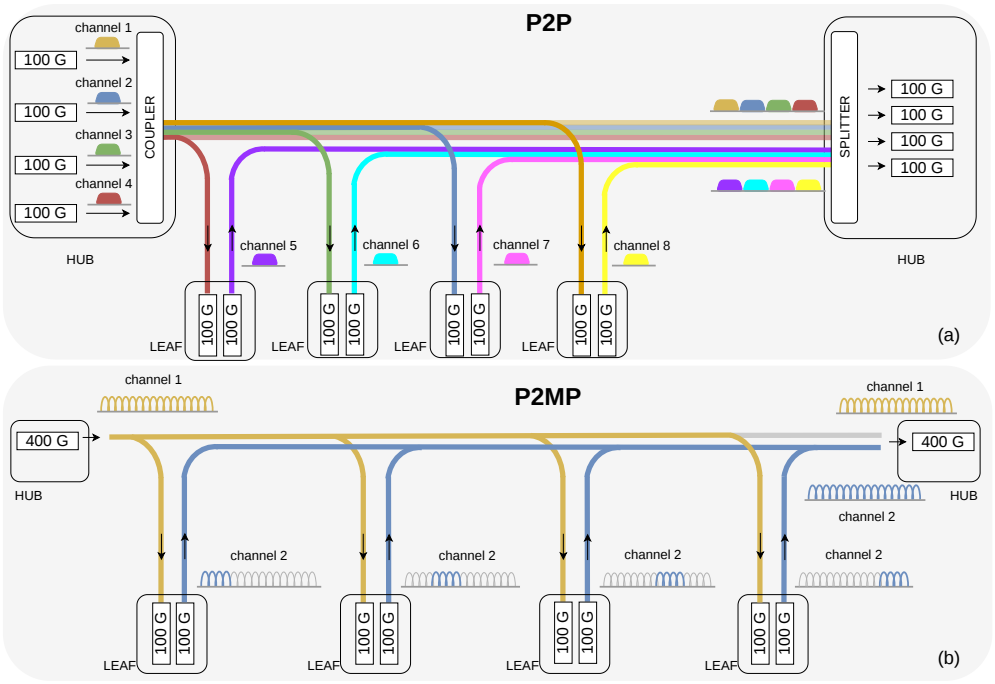

Figure 2. Horseshoe network topology using (**a**) P2P and (**b**) DSCM based P2MP transmission. Each channel is represented by a different color.

Coherent technology plays a crucial role in supporting the substantial capacity growth currently observed in metro networks [34]. Because of their higher power consumption and larger footprint compared with short-reach gray-optics solutions, coherent transceivers have traditionally been deployed as line-card-embedded components within dedicated optical transport systems. Advancements in CMOS process technologies have enabled the emergence of pluggable coherent transceivers, making compact, power-efficient and cost-effective implementations possible [35]. In recent years, multiple MSA initiatives have driven the definition of extended capabilities and improved specifications for coherent pluggable solutions, facilitating their market introduction. The Open ZR+ MSA specifies optical channel formats and details the mapping procedures for 100G, 200G, and 400G Ethernet client signals, enabling the adoption of coherent pluggable optics in QSFP-DD form factor [10]. The Open ROADM MSA adds support of optical transport network (OTN) client signals and can be implemented using either QSFP-DD or CFP2 form factors [11]. The Open XR Optics Forum MSA focuses on P2P- and P2MP-capable coherent pluggable transceivers, considering QSFP-DD and CFP2 modules, aiming to ensure multi-vendor interoperability within an open, multi-source solution [12]. The continuous development of standards and MSA is crucial to meet the industry's increasing demands. For example, the latest Open ZR+ specification (version 3.0) [10] adds high-output transmit power modes (HA and HB), enables support for colorless add/drop configurations, and adopts a higher baud-rate format to extend the operational reach of 400G connections. The 100GBASE-ZR standard in IEEE 802.3 [36] defines the physical layer (PHY) Ethernet specification for 100-Gbps optical transmission implemented using coherent modules in the QSFP28 form factor. This form factor is commonly used for 100-Gbps modules and offers a smaller size and lower power consumption compared to QSFP-DD, which is typically employed for higher-rate coherent interfaces.

3. Network Architecture and Design Methodology

The considered network scenario is presented and an OA optimization methodology tailored to this context is introduced.

3.1. Network Architecture

Figure 3 illustrates the horseshoe FON considered in this work, where the aggregation factor $A = \frac{C_{hub,ch}}{C_{leaf,tot}}$ denotes the ratio between the channel capacity at hub node $C_{hub,ch}$ and the total capacity at a single leaf node $C_{leaf,tot}$. The aggregation factor takes the value one for the case of P2P transmission, whereas it is larger than one when supporting P2MP transmission. The network is based on the typical horseshoe topology, where two hub nodes receive/generate traffic from/to L leaf nodes, ensuring survivability against single-link and single-hub failures. This redundancy requires doubling the number of transceivers: each service demands two transceivers at the leaf node and one transceiver at each hub node. For simplicity, only the propagation from Hub 1 to Hub 2 is depicted in Figure 3, with the optical fiber carrying both DS traffic (Hub 1 to leaf nodes) and US traffic (leaf nodes to Hub 2).

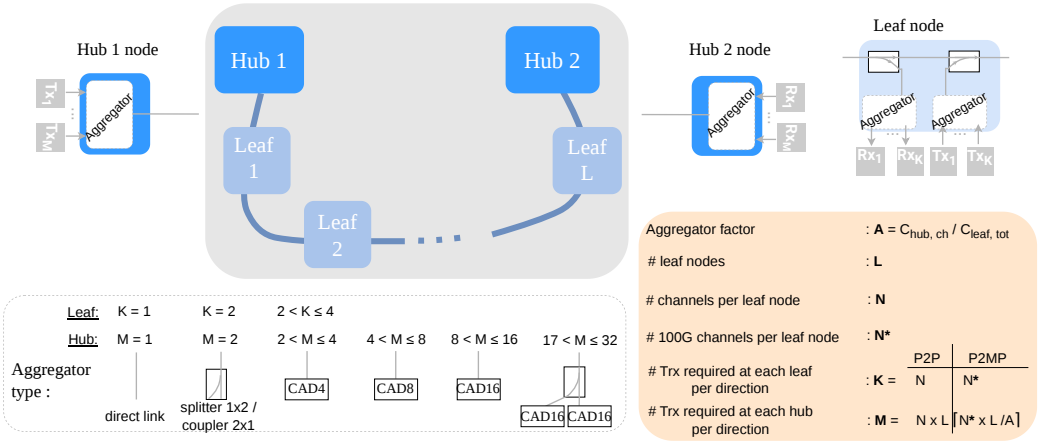

Figure 3. Illustration of a filterless horseshoe network with L leaf nodes, showing the type of aggregation structures for different numbers of transceivers at the hub and leaf nodes.

DS traffic is generated by M transmitters in Hub 1, while US traffic is received by M receivers in Hub 2. In both nodes, an aggregator component/card can be employed for signal combining/broadcasting. At each leaf node, the signal splitting (DS)/merging (US) is performed by a 1×2 splitter/coupler and K transceivers are used to simultaneously transmit and receive K add and K drop signals. An aggregator component/card can be connected to the splitter/coupler to ensure enough add/drop ports are available. OAs are placed at the input and output of each node, acting respectively as pre- and booster amplifiers. QSFP28 pluggable OAs are used as booster and pre-amplifier modules [37] in leaf nodes, whereas QSFP-DD OAs are employed at the hub nodes.

The aggregator architecture, depicted in Figure 3, depends on the number of transceivers: if only a single transceiver is requested, a direct link is sufficient; if two or more transceivers are required, a 1×2 splitter/coupler or a colorless add/drop (CAD) component—assembled by cascading splitters/couplers—is employed. In this study, the maximum K value is 4 (see Figure 3). Therefore, a leaf node may use a direct link, a 1×2 splitter/coupler or a CAD with 4 ports (CAD4). At the hub nodes, a 1×2 splitter/coupler, a CAD with 4/8/16 ports (CAD4/CAD8/CAD16) or a combination of a 1×2 splitter/coupler and two CAD16 when $M > 16$ may be used. The maximum value of M is 32. A quasi-linear transmission regime is imposed by limiting the launch power into each optical fiber, P_{lim}^{max}, to 3 dBm when the transmission of a single carrier or 16SC channel with 64 Gbaud is assumed, corresponding to a -9 dBm threshold per 4 Gbaud

SC, consistent with standard operating conditions for G.652 fibers. Table 1 presents the insertion losses (IL) of CADs, connectors and optical fiber loss, as well as the key characteristics of OAs. The optical fiber length corresponding to the assumed span loss is provided for different optical fiber losses, α, just as a reference. These different lengths correspond to different optical fiber deployments, e.g., longer spans but with lower average loss per kilometer in a rural area or shorter links with higher average loss (due to more frequent splices) in a city center.

Table 1. Component characteristics.

Total span loss	6.25 dB {e.g., 31 km if α = 0.20 dB/km, 25 km if α = 0.25 dB/km, 21 km if α = 0.30 dB/km, 16 km if α = 0.40 dB/km}
Coupler/Splitter	IL: 50/50 = 3.4/3.4 dB; 70/30 = 1.1/5.6 dB
CADs	IL: CAD4 = 6.8 dB; CAD8 = 10.2 dB IL: CAD10 = 11.6 dB; CAD16 = 13.6 dB
Connectors	IL: 0.25 dB
QSFP28 OA	Gain = 9–24 dB Noise Figure = 6.5 dB Saturation power = 17 dBm
QSFP-DD OA	Gain = 9–24 dB Noise Figure = 6.5 dB Saturation power = 21 dBm

3.1.1. Point-to-Point Configuration

In the P2P transmission scenario, each pair of transceivers is configured to a different wavelength, which is occupied in the entire horseshoe (Figure 2a). As illustrated in Figure 3, the number of transceivers required at each leaf node to communicate with a single hub node equals the number of channels supported (N). Consequently, at each hub node, the number of transceivers is given by the number of channels per leaf node (N) multiplied by the number of leaf nodes (L). Importantly, since the FON architecture does not allow the reuse of wavelength channels in non-overlapping paths, the number of DS and US channels supported in each transmission direction of the network cannot exceed the maximum number of channels per optical fiber. For example, $\lceil N \times L/2 \rceil \leq 48$ in the case of using 100 GHz channel spacing and the extended C-band (4.8 GHz). The total number of transceivers deployed in the network is given by $4 \times N \times L$, with a maximum of 192 transceivers required in the case of using all available wavelengths.

3.1.2. Point-to-Multipoint Configuration

In the P2MP based on the DSCM transmission scenario, the leaf nodes' lower-capacity transceivers may receive and transmit one or a group of SCs (Figure 3b). Hence, the capacity of a single channel transmitted/received at a hub node can be efficiently sliced, enabling fine-grained capacity allocation. This work assumes P2MP transceivers are able to slice the optical spectrum into 25G SCs, using 16 quadrature amplitude modulation (DP-16QAM) at ~4 GBd [7]. Particularly, a 400G transceiver is assumed to be used at hub nodes with a total symbol rate of ~64 GBd supporting 16 SCs, whereas the leaf nodes use a 100G transceiver, which can operate at up to 100G via 4 SCs. This corresponds to an aggregation factor $A = 4$. In case each leaf node requires N^* 100G services, the number of 100G transceivers required to communicate with each hub node is N^*. In this scenario, the number of 400G transceivers deployed at each hub node equals $\lceil N^* \times L/4 \rceil$. The advantage of P2MP is

visible when the capacity required per leaf node is significantly smaller than that supported by the high-capacity P2MP transceivers available at the hub nodes. For example, in an eight-leaf node network where each leaf node only demands 100G, using conventional P2P transceivers requires installing a total of 32 × 100G devices, with eight transceivers being deployed in each hub node. Conversely, with P2MP transceivers, a total of 16 × 100G transceivers are still required at leaf nodes, but only 4 × 400G transceivers are required at hub nodes (two transceivers at each hub node), which enables the reduction in cost, power consumption and footprint at the hub nodes [8].

3.2. MSA Pluggable Transceivers

Table 2 summarizes the key specifications of the different coherent pluggable transceiver MSAs: P2P-oriented Open ZR+, Open ROADM and Open XR, defined both for P2P and P2MP. Moreover, in order to gain insight on the impact of the availability of improved implementations of the MSAs (MSAs only indicate the minimum requirements to be compliant), an enhanced Open XR (eOpen XR) transceiver is also considered, which features a slightly improved required OSNR (ROSNR) with respect to the Open XR MSA specification [12]. Given that Open ZR+ HB is the only viable approach for implementing FONs under the Open ZR+ framework, it is adopted as the reference configuration for this MSA. Two types of devices are presented. The first are 400G-capable transceivers, available in QSFP-DD form factor, whereas the second are 100G-capable devices, available in QSFP28 form factor. The first type of devices can trade-off capacity and performance/reach, supporting 400G, 300G and 200G modes, which are realized via signals with a total baud rate that varies between 60 and 64 GBd (depending on the forward error correction code of each MSA), employing 16- and 8-level quadrature amplitude modulation (16QAM and 8QAM) and quadrature phase-shift keying (QPSK), respectively. The second type of device comprises the IEEE 100GBASE-ZR-compliant 100GE [36] transceiver employing QPSK modulation used for P2P deployments and a 100G Open XR QSFP28-optimized transceiver using 16QAM modulation for P2MP transmission. The reported parameters include the IB and OB transmitter OSNR, the maximum Tx output power, the target Rx power, and the ROSNR evaluated at that target Rx power. The IB and OB OSNR values for the 100G ZR QSFP28 modules have been assumed to be compliant with Open ZR+ MSA, while ROSNR has been derived from the vendor's specifications [38]. Since the 100G Open XR QSFP28 has not yet been released, the reported parameters have been reasonably inferred: the Tx side has been modeled using the 100G ZR specifications, while the Rx side has been derived from Open XR characteristics, considering that a 100G rate with 16QAM modulation format uses only 25% of the spectrum of a 400G signal.

Due to the IL of the employed components and the lack of dedicated add/drop OAs, the received power (P_{Rx}) may fall below the target value P_{Rx}^{target}. This reduction can degrade the QoT and is accounted for as a ROSNR penalty. The characterization of this penalty provided by Open ROADM [11] is applied to each of the scenarios considered in Section 4. Figure 4 depicts the ROSNR penalty as a function of the deviation from P_{Rx}^{target}, i.e.,

$$\Delta P_{Rx} = P_{Rx} - P_{Rx}^{target}. \quad (1)$$

Note that, as can be observed in Table 2, modes enabling higher data rates demand higher ROSNR and have a higher target receiver input power, e.g., for the 400G scenario a P_{Rx} of −14 dBm, i.e., a variation from P_{Rx}^{target} of 2 dB, produces a 1 dB ROSNR penalty, whereas there is no ROSNR penalty for lower bit rate scenarios, such as 200G and 300G for the same P_{Rx} of −14 dBm. In view of the transmission distances considered in this network segment, the accumulated chromatic dispersion experienced when using G.652

fiber remains well within the tolerance range supported by the higher-order modes of the considered MSAs.

Table 2. Transceiver characterization.

MSA Standard	Form Factor	IB OSNR [dB]	OB OSNR [dB]	Target Tx pwr. [dBm]	Mode	ROSNR [dB]	Target Rx pwr. [dBm]
Open ZR+ [10]	QSFP-DD	36	43	0	400G 300G 200G	24 21 16	−12 −15 −18
Open ROADM [11]	QSFP-DD	37	36	0	400G 300G 200G	24 21 16	−14 −16 −18
Open XR [12]	QSFP-DD	42	42	0	400G 300G 200G	24 20 15	−12 −16 −17
eOpen XR	QSFP-DD	42	42	0	400G 300G 200G	23 19.5 15	−12 −15 −17
100G ZR	QSFP28	36	43	−4	100G (QPSK)	20.5	−28
100G Open XR	QSFP28	36	43	−4	100G (16QAM)	17	−17

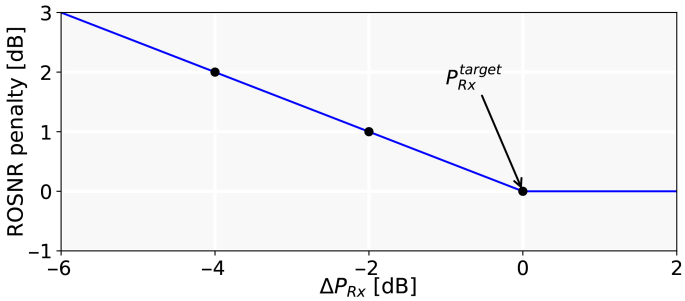

Figure 4. ROSNR penalty as a function of P_{Rx} variation from P_{Rx}^{target}.

3.3. Amplifier Optimization Algorithm

Balancing the optical power of expressed and added signals is desirable to simplify network management and to avoid an additional degradation in the performance of lower power channels. However, this task is non-trivial in FONs due to their filterless nature. Moreover, since downstream (DS) channels, $N_{ch,DS}$, are not blocked, and OB noise, P_{OB}, is not filered out, the saturation power of OAs may be reached rapidly. In fact, OB noise affects not only the QoT of the channels but also the OA total available output power. The OA optimization algorithm described in Figure 5 is proposed to configure the parameters of each OA in the network (i.e., for each i node, the target output power P_{target}, the input power P_{in}, the actual output power P_{out} and the gain G of each pre and boost OA). $N_{ch}(i)$ is the number of channels managed at each node i. For the sake of clarity, the insertion loss of connectors and the steps to calculate the total OB noise are omitted from the description. In the case of the OB noise, we need to account for the contribution of each transceiver to the OB noise from the location where each channel is added up to where the total optical power, or OSNR, is being evaluated. Booster OAs aim to launch the maximum per-channel power into the optical fiber. This value is upper-bounded to mitigate the impact of Kerr non-linearities. The pre-amplifier at each leaf node is used to ensure enough power at the input of the local receivers and to equalize the optical power of channels/SCs at the input of the next booster, unless a specific power imbalance P_{imb} is imposed. Such imbalance may arise from the trade-off between limiting the ROSNR power penalty caused by low Rx power and maintaining similar express and added channel/SC power. When the required OA gain G falls below the specified minimum value G_{min} spec, a variable optical attenuator (VOA) is inserted into the link. Conversely, if the predicted output power exceeds the

saturation threshold (P_{sat}), the gain is clipped to avoid overloading (see the OA setting function in Figure 5). The pre-amplifier in the Rx hub node is configured to ensure the target Rx input power. In cases where a power imbalance is imposed, the OA gain is set based on the channel/SC with the highest power. The main input parameters and decision variables of the algorithm are listed as follows:

Input Parameters:

- P_{Tx}: transceiver output power.
- $IL_{aggr,hub}$, $IL_{aggr,leaf}$: IL of aggregator employed at hub/leaf nodes.
- $IL_{express}$: IL experienced by the expressed signal in the leaf node.
- P_{imb}: power imbalance between expressed and added signals.
- $Link_{loss}(i)$: total link loss in node i.
- $N_{ch,DS}(i)$, $N_{ch,US}(i)$: number of DS/US channels at i node.
- $P_{OB}(i)$: out-of-band noise power.
- P_{lim}^{max}: quasi-linear optical fiber transmission regime power level.
- P_{Rx}^{target}: target Rx power.
- L: number of leaf nodes.

Output Parameters:

- $P_{out}^{pre}(i)$, $P_{out}^{boost}(i)$: pre-/booster OA output power.

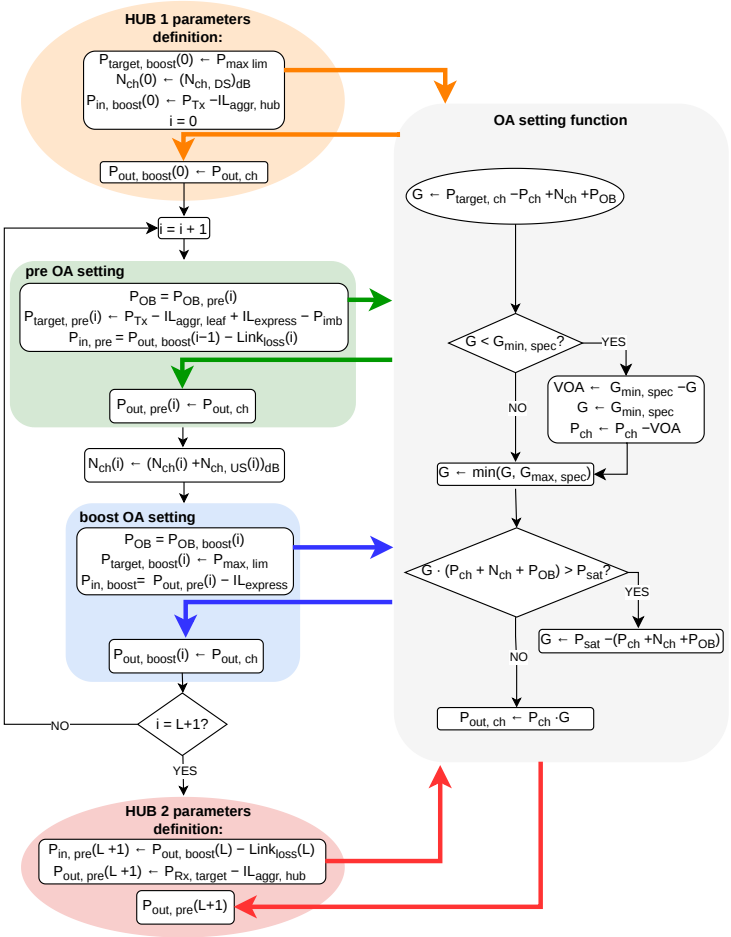

Figure 5. Flowchart of the optimization algorithm for the OAs of a filterless horseshoe network. Each building block is identified by a different color.

Note that the computational complexity of the proposed algorithm scales linearly with the network size, since the optimization is executed independently and only once for each network node.

4. Results and Discussion

This section reports a comprehensive assessment of the scalability of filterless horseshoe networks employing different interoperable coherent pluggable transceivers. The QoT estimator used in our analysis is the residual margin (RM) at the receiver, defined for a given path as

$$RM = OSNR - ROSNR(P_{Rx}) - S, \quad (2)$$

where OSNR denotes the available OSNR at the receiver input, measured in a reference optical noise bandwidth of 0.1 nm, and is given by the ratio between the signal power P_{signal} and total noise power, $P_{ASE,\,tot}$: $OSNR = P_{signal}/P_{ASE,\,tot}$. The noise power accounts for the contributions of IB noise, OB noise arising in the remaining channels, and ASE noise from OAs. A system margin, S, is set to 1 dB in this work to account for factors that can impact performance (e.g., fiber and component aging). The ROSNR for a given receiver input power P_{Rx} is defined by the selected MSA, the channel mode considered, and the power penalty (see Table 2 and Figure 4). The RM must be equal to or greater than zero for a channel to be feasible. Two different network scenarios have been considered: a high-capacity scenario and a low-capacity scenario. The former is supported by the P2P configuration, and the design assumes that a maximum rate of 400 Gbps per channel is targeted. If the channel cannot be supported due to insufficient QoT, the rate is stepped down to 300 Gbps and, if necessary, to 200 Gbps. The procedure is repeated until a valid operating point is identified, guaranteeing that the DS and US transmission directions run at the same rate on both fibers. Open ZR+, Open ROADM and Open XR compliant transceivers could be considered for deployment in our analysis. However, due to the low OB OSNR requirement defined in the Open ROADM standard, it was observed that this MSA is not suitable for FONs, and it is, therefore, omitted from the subsequent analysis to improve readability. The low-capacity scenario accommodates both P2P and P2MP architectures. The maximum target rate per channel is set to 100 Gbps, which results in the use of 100G ZR transceivers for the P2P case and 400G/100G Open XR transceivers for the P2MP case. The detailed scalability assessment of the described architectures and MSA-compliant transceivers is performed by: (i) increasing the number of leaf nodes—and consequently also the number of transceivers and channels—across the network; and (ii) expanding the number of transceivers N (in P2P case) or N^* (in P2MP case) per leaf node for the same number of leaf nodes, L.

4.1. High-Capacity Network Scenario

Figure 6 presents the RM at each receiver of a FON with $L = 4$ leaf nodes and four channels per leaf node ($N = 4$), where the OAs are simply configured following the intuitive approach of meeting the target power at the deployed Open ZR+ HB transceivers. To attain the P_{Rx}^{target}, the expressed signal is transmitted with a higher signal power than the added signal. Consequently, and due to the limited optical power equalization in leaf nodes, this configuration introduces a power imbalance of 2.8 dB between expressed and added signals. Thus, the expressed and added signals (and noise) are merged with different power levels, with the lower-power channels becoming more impacted by the noise accumulated throughout the network. To highlight this effect, the RM analysis reported in Figure 6 considers not only the case where OB noise is present but also the case where it is neglected (e.g., if channels were filtered). This allows us to observe (i) the importance of correctly

modeling the impact of OB noise in FONs and (ii) setting the pre-amplifiers as to achieve a compromise between maximizing the input power of the local receivers and balancing the power of expressed and locally added channels since, as can be observed, only 300G channels can be supported in this case due to the 3 dB lower ROSNR, whereas in a filtered network, 400G channels would be viable.

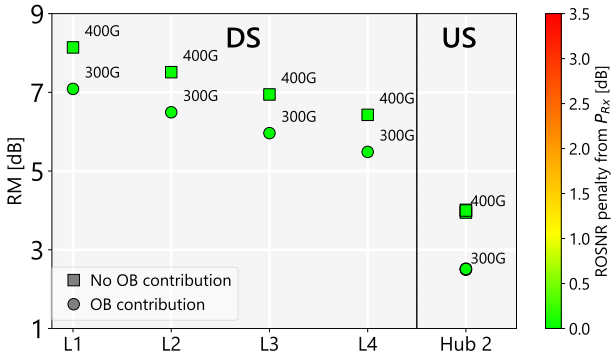

Figure 6. RM at each leaf node with and without considering the impact of OB noise.

As shown by the triangle results in Figure 7a, when applying the optimization algorithm described in Figure 5, the network attains its maximum total capacity (i.e., each channel uses the 400G mode), although there is a ROSNR penalty with respect to simply meeting the P_{Rx}^{target} at the receiver (scenario depicted by circles) due to the reduced input power at the receivers in the DS transmission direction. Moreover, to achieve the same target launch power per channel as in the reference scenario, the booster gain increases, resulting in a QoT degradation in the subsequent leaf nodes. The network can scale up to six channels per leaf node ($N = 6$), constrained by the FON's inability to reuse wavelengths on disjoint paths. In this scenario, aggregator cards with higher IL are required, further reducing the power available at the input of the receivers. This increases the ROSNR penalty and consequently degrades the network performance and capacity (squares in Figure 7b). In this case, some of the leaf nodes need to operate in 200G mode in DS, which forces the US to operate at the same rate. As a consequence, two different operating modes are required in the US direction (i.e., two different squares in the US area of the graph). This limitation can be mitigated by using unbalanced splitter/couplers. As shown by the reverted triangles in Figure 7b, adopting a 30/70 (express/drop) splitting ratio followed by a 30/70 (express/add) coupling ratio enables the network to achieve a higher total capacity, since all connections can be established with the 300G mode.

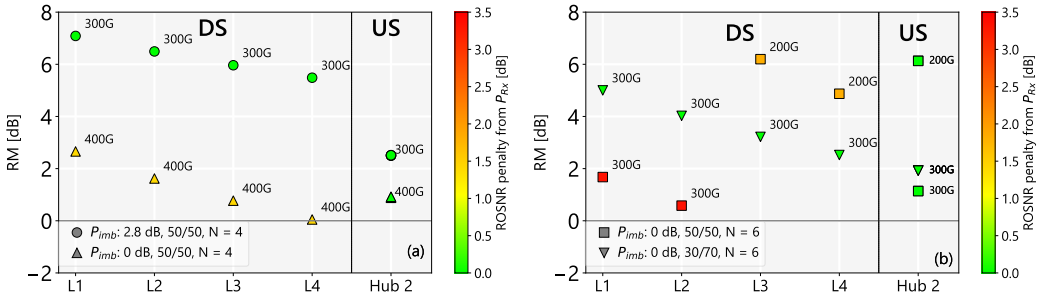

Figure 7. Analysis of RM [dB] when deploying Open ZR+ HB pluggables as a function of (**a**) power imbalance (**b**) splitter ratio in FON OADM.

As shown in Figure 8a, when scaling the network to support a larger number of leaf nodes $L = 8$, the maximum total capacity can be achieved with up to two channels per leaf node ($N = 2$). Note that the constraint on wavelength reuse limits the maximum number of channels per leaf node to three ($N = 3$). Figure 8b depicts the optical noise-to-signal

ratio (ONSR) percentage, discriminating the ASE noise and the IB/OB noise contributions. As can be observed, the IB/OB noise generated by the transmitters is the dominant source of noise in this scenario, that is, with $L = 8$ and for both $N = 2$ and $N = 3$. The higher ONSR with $N = 3$ limits the per-channel capacity to 300G in this case.

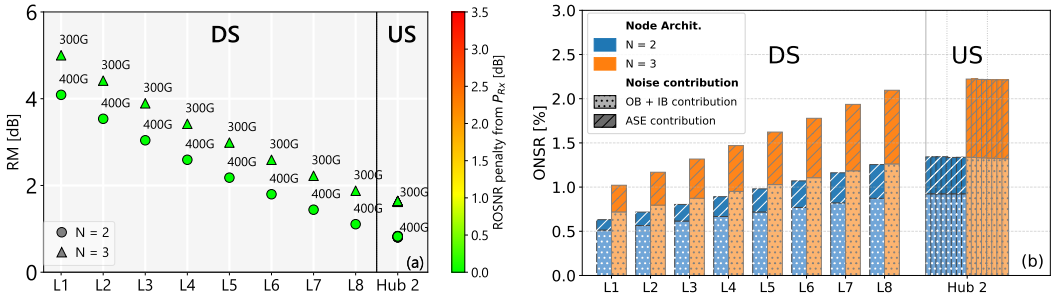

Figure 8. 8-leaf node FON with $N = 2$ vs $N = 3$: (**a**) RM results and (**b**) ONSR results.

4.2. Low-Capacity Network Scenario

As introduced before, in cases with lower capacity, e.g., where each leaf node may need only up to 100G capacity, two main deployment scenarios can be envisioned. The first consists of using lower-capacity P2P transceivers, whereas the second comprises a combination of higher-capacity P2MP transceivers at the hub nodes with lower-capacity P2MP transceivers at the leaf nodes. For the case of P2P transceivers, two deployment scenarios are modeled: the first consists of using 100G ZR transceivers at both hub and leaf nodes, whereas the second uses instead Open XR 100G devices. By comparing the results obtained in these two scenarios, it is possible to gain insight on the performance impact of transceivers that are based on two different MSAs. P2MP transmission is realized using Open XR 400G transceivers at the hub nodes and Open XR 100G transceivers at the leaf nodes. Comparing the results obtained with P2MP with those from using P2P with Open XR 100G transceivers allows us to understand the potential improvements from adopting a P2MP transmission solution.

Figure 9 shows the RM and ONSR results obtained with P2P and P2MP transceivers for two configurations of a horseshoe network: (1) $L = 4$ with N (in the P2P case) and N^* (in the P2MP case) equal to 1; (2) $L = 8$ and N or N^* equal to 3. All the design results were obtained by employing the proposed OA settings optimization algorithm described in Section 3.3.

The results for $L = 4$ provide evidence of the superiority of 100G devices that are compliant with the Open XR MSA over those compliant with 100G ZR, as can be seen from the higher RM and the lower ONSR. Note that, in both cases, the number of transceivers deployed is the same, and the insertion losses experienced by the optical signals along their paths are also the same. Hence, the performance advantage of Open XR 100G devices is solely due to the improved specifications (e.g., the same -4 dBm Tx output power is allocated to a 4×4 Gbaud signal instead of to a 30 Gbaud signal). Nevertheless, it should be noticed that meeting improved specifications may result in an increase in device cost. The other key observation of the comparative results is the clear superiority of the P2MP transmission solution, particularly in the DS transmission direction. In this case, besides the savings enabled by replacing four 100G transceivers at each hub node by a single 400G transceiver, lowering cost, power consumption and footprint, there are two benefits arising from the fact that the 400G transceiver can be directly connected to the booster amplifier, whereas the four 100G transceivers are connected to a CAD4. The first benefit is the lower insertion losses experienced by the signals added (and dropped) at the hub nodes, enabling the reduction in amplifier gain and, hence, the ASE noise generated. The second benefit is that in the process of aggregating the four 100G signals with a CAD4, each signal generates

OB noise that cumulatively impacts the other signals, which does not occur with the single 400G device. This is visible in the ONSR results shown in Figure 9c.

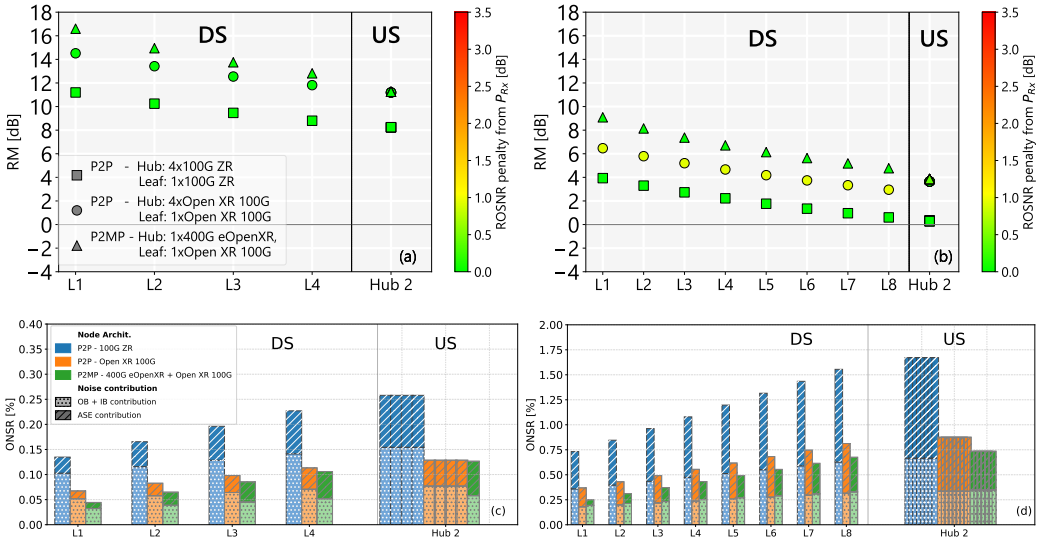

Figure 9. Comparison of P2P and P2MP architectures for $L = 4$ with N (P2P) and N^* (P2MP) equal to 1 (**a**), $L = 8$ with N (P2P) and N^* (P2MP) equal to 3 (**b**), and their corresponding noise contributions (**c**,**d**).

The same analysis for $L = 8$ and N or N^* equal to 3 is reported in Figure 9b for the RM and Figure 9d for the ONSR. These results reinforce the trends identified in the smaller horseshoe network with fewer channels. For instance, the benefits in RM improvement from adopting a P2MP transmission solution become even more evident. Note that, when the optimization algorithm introduced in Section 3.3 is applied, balancing express and added channel powers, the ROSNR input power penalty will be higher with the Open XR 100G, because the 100G mode with 16QAM modulation format has a higher target Rx power than the 100G mode with QPSK used in 100G ZR. This is visible with the yellow coloring of the circle markers. The described penalty is avoided at Hub 2, since the pre-amplifier can operate with higher gain (all channels are locally dropped).

Note that in all evaluated scenarios, the total optimization time was shorter than 1 s, using a 13th Gen Intel(R) Core(TM) i7-1355U CPU and a 32.0 GB memory RAM, highlighting the scalability of the proposed optimization algorithm.

5. Conclusions

This work presented a comprehensive analysis of filterless horseshoe networks operating with modern coherent pluggable transceivers under both high- and low-capacity scenarios, evaluating P2P and P2MP transmission solutions. The study highlighted the major design challenges arising from the filterless nature of FONs—namely spectrum waste, limited equalization capabilities in intermediate nodes, and noise accumulation—while quantifying the specific impact of transmitter out-of-band noise. The results demonstrated that OB noise plays a critical role in determining the performance, and consequently scalability, of filterless horseshoe networks. In high-capacity P2P deployments, OB noise significantly reduces the achievable RM, directly impacting system capacity. An optimization algorithm for OA settings was proposed and shown to mitigate part of this degradation by balancing expressed and added signal power. Nevertheless, as the node count or the number of channels per leaf node increases, the impact of ASE and OB/IB noise contributions ultimately limits scalability. The analysis also revealed that the traditional symmetric splitter/coupler configurations may not provide sufficient performance at larger scales.

Employing unbalanced splitting ratios (e.g., 30/70) was shown to effectively improve received power, as well as reduce ROSNR penalties. In low-capacity scenarios, P2MP emerges as a particularly advantageous transmission solution. The reduced OB contribution and lower insertion loss at hub nodes allow P2MP links to achieve higher RM and improved scalability compared with conventional P2P solutions. This was confirmed in both 4- and 8-leaf-node networks, where P2MP consistently achieved superior performance. Overall, the study confirms that FONs combined with MSA-compliant coherent pluggable transceivers can serve as cost-effective and scalable solutions for metro-aggregation and metro-access networks. However, OB noise, power imbalance, and wavelength-reuse constraints impose practical limitations that must be carefully addressed through optimized OA configurations, appropriate splitter designs, and MSAs selection.

Author Contributions: Conceptualization, F.G., J.P. and N.C.; Methodology, F.G., J.P., N.C. and L.C.; Software, F.G.; Validation, N.C.; Investigation, F.G., J.P. and N.C.; Writing—original draft, F.G.; Writing—review & editing, F.G., J.P., N.C. and L.C.; Supervision, J.P. and L.C. All authors have read and agreed to the published version of the manuscript.

Funding: This project has received funding from the European Union's Horizon Europe research and innovation programme under the Marie Skłodowska-Curie Doctoral Network (MSCA-DN) NESTOR, Grant Agreement No. 101119983, EU Horizon Europe research and innovation programme under GA 101092766 (ALLEGRO), by national funds through FCT—Fundacão para a Ciência e a Tecnologia, I.P., and, when eligible, co-funded by EU funds under project/support UID/50008/2025—Instituto de Telecomunicacões, DOI:10.54499/UID/50008/2025.

Data Availability Statement: Data are contained within the article.

Conflicts of Interest: Author Federica Gatti, João Pedro, Nelson Costa were employed by the company Nokia. The remaining authors declare that the research was conducted in the absence of any commercial or financial relationships that could be construed as a potential conflict of interest.

References

1. Baziana, P.; Drainakis, G.; Georgantas, D.; Bogris, A. AI and ML Applications Traffic: Designing Challenges for Performance Optimization of Optical Data Center Networks. In Proceedings of the 2024 International Conference on Software, Telecommunications and Computer Networks (SoftCOM), Split, Croatia, 26–28 September 2024; pp. 1–6. [CrossRef]
2. Nokia Global Network Traffic Report. Available online: https://onestore.nokia.com/asset/213660 (accessed on 18 February 2026).
3. Eira, A.; Costa, N.; Pedro, J. On the Capacity and Scalability of Metro Transport Architectures for Ubiquitous Service Delivery. In *2018 20th International Conference on Transparent Optical Networks (ICTON)*; IEEE: Piscataway, NJ, USA, 2018.
4. Hosseini, M.M.; Pedro, J.; Napoli, A.; Costa, N.; Prilepsky, J.E.; Turitsyn, S.K. Optimization of survivable filterless optical networks exploiting digital subcarrier multiplexing. *J. Opt. Commun. Netw.* **2022**, *14*, 586–594. [CrossRef]
5. Ibrahimi, M.; Ayoub, O.; Karandin, O.; Musumeci, F.; Castoldi, A.; Pastorelli, R.; Tornatore, M. QoT-Aware Optical Amplifier Placement in Filterless Metro Networks. *IEEE Commun. Lett.* **2021**, *25*, 931–935. [CrossRef]
6. Karandin, O.; Ayoub, O.; Ibrahimi, M.; Castoldi, A.; Pastorelli, R.; Musumeci, F.; Tornatore, M. Design with low cost of equipment for metro filterless optical networks. *J. Opt. Commun. Netw.* **2025**, *17*, 198–208. [CrossRef]
7. Welch, D.; Napoli, A.; Back, J.; Sande, W.; Pedro, J.; Masoud, F.; Fludger, C.; Duthel, T.; Sun, H.; Hand, S.J.; et al. Point-to-Multipoint Optical Networks Using Coherent Digital Subcarriers. *J. Light. Technol.* **2021**, *39*, 5232–5247. [CrossRef]
8. Back, J.; Wright, P.; Ambrose, J.; Chase, A.; Jary, M.; Masoud, F.; Sugden, N.; Wardrop, G.; Napoli, A.; Pedro, J.; et al. CAPEX Savings Enabled by Point-to-Multipoint Coherent Pluggable Optics Using Digital Subcarrier Multiplexing in Metro Aggregation Networks. In *Proceedings of the 2020 European Conference on Optical Communications (ECOC)*; IEEE: Piscataway, NJ, USA, 2020. [CrossRef]
9. Hosseini, M.M.; Pedro, J.; Napoli, A.; Costa, N.; Prilepsky, J.E.; Turitsyn, S.K. Multi-period planning in metro-aggregation networks exploiting point-to-multipoint coherent transceivers. *J. Opt. Commun. Netw.* **2023**, *15*, 155–162. [CrossRef]
10. Open ZR+ MSA Technical Specifications. Available online: https://openzrplus.org/wp-content/uploads/2024/04/openzrplus_rev3p0_final2.pdf (accessed on 18 February 2026).

11. Open ROADM MSA Technical Specifications. Available online: https://view.officeapps.live.com/op/view.aspx?src=https%3A%2F%2Fraw.githubusercontent.com%2Fwiki%2FOpenROADM%2FOpenROADM_MSA_Public%2Ffiles%2F20250327_open-roadm_msa_specification_ver8.0.1.xlsx&wdOrigin=BROWSELINK (accessed on 18 February 2026).
12. Open XR MSA Technical Specifications. Available online: https://static1.squarespace.com/static/60ad0ce2e5c6877a569c6a59/t/68ca8e91aa68bc4840c5587f/1758105233694/Open+XR+Optics+Transceiver+Optical+and+Client+Interface+Specification+02.pdf (accessed on 18 February 2026).
13. Tremblay, C.; Littlewood, P.; Bélanger, M.P.; Wosinska, L.; Chen, J. Agile filterless optical networking. In Proceedings of the 2017 International Conference on Optical Network Design and Modeling (ONDM), Budapest, Hungary, 15–18 May 2017; pp. 1–4. [CrossRef]
14. Tremblay, C. Overview of the research work on filterless optical networking. Invited talk, 2015. Presented at the Deutsche Telekom, Darmstadt, Germany, 4 May 2015.
15. Tremblay, C.; Archambault, E.; Wilson, R.G.; Clelland, S.; Furdek, M.; Wosinska, L. Agile Metropolitan Filterless Optical Networking. In Proceedings of the 2022 IEEE Future Networks World Forum (FNWF), Montreal, QC, Canada, 12–14 October 2022; pp. 113–116. [CrossRef]
16. Tremblay, C.; Archambault, E.; Wilson, R.G.; Clelland, S.; Furdek, M.; Wosinska, L. Cost- and energy-efficient filterless architectures for metropolitan networks. *J. Opt. Commun. Netw.* **2023**, *15*, D47–D55. [CrossRef]
17. Tremblay, C.; Archambault, E.; Belanger, M.P.; Littlewood, P.; Clelland, W.; Furdek, M.; Wosinska, L. Agile Optical Networking: Beyond Filtered Solutions. In *Proceedings of the Optical Fiber Communication Conference, San Diego, CA, USA, 11–15 March 2018*; Optica Publishing Group: Washington, DC, USA, 2018; p. M1A.5. [CrossRef]
18. Ayoub, O.; Karandin, O.; Ibrahimi, M.; Castoldi, A.; Musumeci, F.; Tornatore, M. Tutorial on Filterless Optical Networks [Invited]. *J. Opt. Commun. Netw.* **2022**, *14*, 1–15. [CrossRef]
19. Archambault, E.; Alloune, N.; Furdek, M.; Xu, Z.; Tremblay, C.; Muhammad, A.; Chen, J.; Wosinska, L.; Littlewood, P.; Belanger, M.P. Routing and Spectrum Assignment in Elastic Filterless Optical Networks. *IEEE/ACM Trans. Netw.* **2016**, *24*, 3578–3592. [CrossRef]
20. Etezadi, E.; Natalino, C.; Tremblay, C.; Wosinska, L.; Furdek, M. Programmable Filterless Optical Networks: Architecture, Design, and Resource Allocation. *IEEE/ACM Trans. Netw.* **2024**, *32*, 1096–1109. [CrossRef]
21. Furdek, M.; Muhammad, A.; Zervas, G.; Alloune, N.; Tremblay, C.; Wosinska, L. Programmable filterless network architecture based on optical white boxes. In Proceedings of the 2016 International Conference on Optical Network Design and Modeling (ONDM), Cartagena, Spain, 9–12 May 2016; pp. 1–6. [CrossRef]
22. Ayoub, O.; Fatima, F.; Bovio, A.; Musumeci, F.; Tornatore, M. Traffic-Adaptive Re-Configuration of Programmable Filterless Optical Networks. In Proceedings of the ICC 2020–2020 IEEE International Conference on Communications (ICC), Virtually, 7–11 June 2020; pp. 1–6. [CrossRef]
23. Karandin, O.; Ayoub, O.; Ibrahimi, M.; Musumeci, F.; Castoldi, A.; Pastorelli, R.; Tornatore, M. Optical Metro Network Design with Low Cost of Equipment. In Proceedings of the 2021 International Conference on Optical Network Design and Modeling (ONDM), Gothenburg, Sweden, 28 June 28–1 July 2021; pp. 1–4. [CrossRef]
24. Xu, Z.; Archambault, E.; Tremblay, C.; Chen, J.; Wosinska, L.; Belanger, M.P.; Littlewood, P. 1+1 Dedicated Optical-Layer Protection Strategy for Filterless Optical Networks. *IEEE Commun. Lett.* **2014**, *18*, 98–101. [CrossRef]
25. Ibrahimi, M.; Ayoub, O.; Albanese, F.; Musumeci, F.; Tornatore, M. Strategies for Dedicated Path Protection in Filterless Optical Networks. In Proceedings of the 2021 IEEE Global Communications Conference (GLOBECOM), Madrid, Spain, 7–11 December 2021; pp. 1–6. [CrossRef]
26. Ibrahimi, M.; Ayoub, O.; Attarpour, A.; Musumeci, F.; Castoldi, A.; Ragni, M.; Tornatore, M. Minimizing equipment and energy cost in mixed 10G and 100G/200G filterless horseshoe networks with hierarchical OTN boards. *Ann. Telecommun.* **2023**, *78*, 297–311. [CrossRef]
27. Chen, J.; Khanmohamadi, S.; Abtahi, F.; Wosinska, L.; Xu, Z.; Cassidy, A.; Tremblay, C.; Littlewood, P.; Asselin, S.; Bélanger, M.P. Passive wide area network solutions: Filterless and semi-filterless optical networks. In Proceedings of the 2011 13th International Conference on Transparent Optical Networks, Stockholm, Sweden, 26–30 June 2011; p. 1. [CrossRef]
28. Khanmohamadi, S.; Chen, J.; Abtahi, F.; Wosinska, L.; Cassidy, A.; Archambault, E.; Tremblay, C.; Asselin, S.; Littlewood, P.; Bélanger, M. Semi-filterless optical network: A cost-efficient passive wide area network solution with effective resource utilization. In Proceedings of the 2011 Asia Communications and Photonics Conference and Exhibition (ACP), Shanghai, China, 13–16 November 2011; pp. 1–3.
29. Ayoub, O.; Shehata, S.; Musumeci, F.; Tornatore, M. Filterless and Semi-Filterless Solutions in a Metro-HAUL Network Architecture. In Proceedings of the 2018 20th International Conference on Transparent Optical Networks (ICTON), Bucharest, Romania, 1–5 July 2018; pp. 1–4. [CrossRef]

30. Castro, C.; Napoli, A.; Porrega, M.; Back, J.; Rashidinejad, A.; Quagliotti, M.; Riccardi, E.; Hillerkuss, D.; Yekani, A.; Masoud, F.; et al. Scalable filterless coherent point-to-multipoint metro network architecture. *J. Opt. Commun. Netw.* **2023**, *15*, B53–B63. [CrossRef]
31. Hosseini, M.M.; Pedro, J.; Napoli, A.; Costa, N.; Prilepsky, J.E.; Turitsyn, S.K. Optimized design of filterless horseshoe networks exploiting point-to-multipoint coherent transceivers. *J. Opt. Commun. Netw.* **2023**, *15*, 569–582. [CrossRef]
32. Hosseini, M.M.; Pedro, J.; Costa, N.; Castro, C.; Napoli, A. Optimized design of horseshoe-and-spur filterless networks leveraging point-to-multipoint coherent pluggable transceivers. *J. Opt. Commun. Netw.* **2024**, *16*, 969–983. [CrossRef]
33. Hosseini, M.M.; Parisi, G.; Pedro, J.; Torres-Ferrera, P.; Napoli, A. Low-Nonlinearity-Margin Design of Filterless Horseshoe-and-Spur Networks. In Proceedings of the Optical Fiber Communication Conference (OFC) 2025, San Francisco, CA, USA, 30 March–3 April 2025.
34. Pedro, J. Networking Benefits of Coherent Pluggable Optics. In *Proceedings of the Optical Fiber Communication Conference (OFC) 2024*; Optica Publishing Group: Washington, DC, USA, 2024; p. W3C.2. [CrossRef]
35. Pedro, J.; Hosseini, M.M.; Napoli, A. Extended network applications of coherent pluggable transceivers [Invited]. *J. Opt. Commun. Netw.* **2025**, *17*, A210–A223. [CrossRef]
36. *IEEE Standard 802.3-2022 (Revision of IEEE Standard 802.3-2018)*; IEEE Standard for Ethernet. IEEE: Piscataway, NJ, USA, 2022; pp. 1–7025 . [CrossRef]
37. Edge-Core Packet Optical Pluggable EDFA. Available online: https://www.edge-core.com/_upload/images/2022-069-Packet-Optical-EDFA-DS-R02-20221121.pdf#: :text=The%20modules%20are%20designed%20for%20packet-optical%2C%20low-cost%2C%20reduced,need%20of%20using%20an%20expensive%20open%20line%20system (accessed on 18 February 2026).
38. ADVA Coherent Pluggable 100G ZR. Available online: https://www.adtran-networks.com/-/media/adva-main-site/resources/data-sheets/pdfs/coherent-100zr.pdf (accessed on 18 February 2026).